The Astrophysical Journal, 922:35 (9pp), 2021 November 20 https://doi.org/10.3847/1538-4357/ac142b
© 2021. The American Astronomical Society. All rights reserved.

The Green Bank Northern Celestial Cap Pulsar Survey. VI. Discovery and Timing of PSR J1759+5036: A Double Neutron Star Binary Pulsar

G. Y. Agazie[1,2,3], M. G. Mingyar[1,2,4], M. A. McLaughlin[1,2], J. K. Swiggum[5], D. L. Kaplan[3], H. Blumer[1,2], P. Chawla[6], M. DeCesar[5], P. B. Demorest[7], W. Fiore[1,2], E. Fonseca[6], J. D. Gelfand[8,9], V. M. Kaspi[6], V. I. Kondratiev[10], M. LaRose[1,2], J. van Leeuwen[10], L. Levin[11], E. F. Lewis[1,2], R. S. Lynch[12], A. E. McEwen[3], H. Al Noori[13], E. Parent[6], S. M. Ransom[14], M. S. E. Roberts[8,15], A. Schmiedekamp[16], C. Schmiedekamp[16], X. Siemens[17], R. Spiewak[11,18], I. H. Stairs[19], and M. Surnis[11]

[1] Department of Physics and Astronomy, West Virginia University, Morgantown, WV 26501, USA; gyagazie@uwm.edu
[2] Center for Gravitational Waves and Cosmology, West Virginia University, Chestnut Ridge Research Building, Morgantown, WV 26505, USA
[3] Center for Gravitation, Cosmology, and Astrophysics, Dept. of Physics, University of Wisconsin-Milwaukee, P.O. Box 413, Milwaukee, WI 53201, USA
[4] Department of Physics, Montana State University, Bozeman, MT, 59717, USA
[5] Department of Physics, 730 High St., Lafayette College, Easton, PA 18042, USA
[6] Department of Physics and McGill Space Institute, McGill University, Montreal, QC H3A 2T8, Canada
[7] National Radio Astronomy Observatory, P.O. Box O, Socorro, NM 87801, USA
[8] Center for Astro, Particle, and Planetary Physics, New York University Abu Dhabi, PO Box 129188, Abu Dhabi, UAE
[9] Affiliated Member, Center for Cosmology and Particle Physics, New York University, New York, NY, 10276, USA
[10] ASTRON, the Netherlands Institute for Radio Astronomy, Oude Hoogeveensedijk 4, 7991 PD Dwingeloo, The Netherlands
[11] Jodrell Bank Centre for Astrophysics, School of Physics and Astronomy, The University of Manchester, Manchester, M13 9PL, UK
[12] Green Bank Observatory, P.O. Box 2, Green Bank, WV 24494, USA
[13] Deptarment of Physics, University of California, Santa Barbara, CA 93106, USA
[14] National Radio Astronomy Observatory, 520 Edgemont Road, Charlottesville, VA 22903, USA
[15] Eureka Scientific, Inc., 2452 Delmer Street, Suite 100, Oakland, CA 94602, USA
[16] Department of Physics, The Pennsylvania State University, Ogontz Campus, Abington, Pennsylvania 19001, USA
[17] Department of Physics, Oregon State University, Corvallis, OR 97331, USA
[18] Centre for Astrophysics and Supercomputing, Swinburne University of Technology, P.O. Box 218, Hawthorn, VIC 3122, Australia
[19] Department of Physics and Astronomy, University of British Columbia, 6224 Agricultural Road, Vancouver, BC V6T 1Z1 Canada
Received 2021 February 19; revised 2021 July 6; accepted 2021 July 12; published 2021 November 16

Abstract

The Green Bank North Celestial Cap survey is a 350 MHz all-sky survey for pulsars and fast radio transients using the Robert C. Byrd Green Bank Telescope. To date, the survey has discovered over 190 pulsars, including 33 millisecond pulsars and 24 rotating radio transients. Several exotic pulsars have been discovered in the survey, including PSR J1759+5036, a binary pulsar with a 176 ms spin period in an orbit with a period of 2.04 days, an eccentricity of 0.3, and a projected semi-major axis of 6.8 light seconds. Using seven years of timing data, we are able to measure one post–Keplerian parameter, advance of periastron, which has allowed us to constrain the total system mass to $2.62 \pm 0.03\,M_{\odot}$. This constraint, along with the spin period and orbital parameters, suggests that this is a double neutron star system, although we cannot entirely rule out a pulsar-white dwarf binary. This pulsar is only detectable in roughly 45% of observations, most likely due to scintillation. However, additional observations are required to determine whether there may be other contributing effects.

Unified Astronomy Thesaurus concepts: Binary pulsars (153); Pulsars (1306); Radio pulsars (1353); Neutron stars (1108)

1. Introduction

The Green Bank North Celestial Cap (GBNCC) pulsar survey[20] is a comprehensive survey of the northern celestial sky ($\delta > -40°$) at 350 MHz (Stovall et al. 2014) with the Robert C. Byrd Green Bank Telescope (GBT) in West Virginia. The GBNCC survey is projected to cover ∼80% of the entire sky with sensitivity to millisecond pulsars (MSPs), canonical pulsars, and sources of isolated dispersed pulses such as rotating radio transients (RRATs) and fast radio bursts (FRBs) (McLaughlin et al. 2006; Lorimer et al. 2007; Thornton et al. 2013). The nominal sensitivity to pulsars is 0.74 mJy with an 6% duty cycle, which corresponds to a dispersion measure (DM) of 0 pc cm^{-3}, spin period of ∼1 s, and sky temperature of 95 K, as shown in Figure 3 of McEwen et al. (2020).

Pulsars with a binary companion comprise about 6% of all known pulsars (ATNF Pulsar Catalogue v1.63; Manchester et al. 2005). Most MSPs are in binary systems, as they are spun-up to millisecond periods through angular momentum transfer from a companion through Roche Lobe overflow (Alpar et al. 1982; Lorimer 2008). This accretion process typically results in an MSP-white dwarf system in an extremely circular orbit, with eccentricity of $10^{-5} \lessapprox e \lessapprox 0.01$ (Phinney 1992).

Some binary pulsars take a different evolutionary track. If the companion is massive enough to also undergo a supernova, and the kick of both explosions does not destabilize and break up the system, then a double neutron star (DNS) binary will result (e.g., Tauris et al. 2017). In this case, the first-born neutron star will be "recycled," and the second-born neutron star will be a canonical pulsar. It has been observed that recycled DNS pulsars have spin periods (P) ranging from 16.9 ms to 185 ms and period derivative ($\dot{P}$) range of 2.2×10^{-20}–1.7×10^{-17} s s^{-1} (Manchester et al. 2005; Tauris et al. 2017; Pol et al. 2019).

[20] http://astro.phys.wvu.edu/GBNCC/

Table 1
Summary of Observations for PSR J1759+5036 with the Number of Observations (N_{obs}), Observing Frequencies, and Detections per Observation Run Indicated

Time frame	Frequency (MHz)	N_{obs}	Detections
2013–2014	820	24	10
2017–2019	820/350	54	20
2019/10	350	7	5
2019/12–2020/01	820	24	15

Currently, 15 DNS systems are known; in 13 of them, we have detected the recycled pulsar, with P ranging from 16.9 ms to 185 ms (Pol et al. 2019). In two systems, however, the younger canonical pulsar has been detected, with P of 144 ms and 2.7 s, and $\dot{P}$ of 2.0×10^{-14} s s^{-1} and 8.9×10^{-16} s s^{-1}, respectively. The DNS systems have eccentricities ranging from 0.08 to 0.83 (ATNF Pulsar Catalogue v1.63; Manchester et al. 2005). Some DNS systems have a measurable post-Keplerian (PK) parameter, which can be used to place constraints on the total system, pulsar, and companion masses. Measurement of two PK parameters can fully constrain the pulsar and companion masses and other system parameters such as orbital inclination (Damour & Deruelle 1985; Taylor & Weisberg 1989; Damour & Taylor 1992). A third makes the system overdetermined, meaning it can be used to test theories of gravity by calculating the predicted value for the third PK parameter given the first two and comparing it to the measured value (Stairs 2003; Kramer et al. 2006).

In this paper, we report the discovery and properties of PSR J1759+5036, a 176 ms binary pulsar in a two day, eccentric orbit. Its small $\dot{P}$ suggests partial recycling, which is consistent with the properties of DNS systems. We present evidence, including a mass constraint, to suggest this system is likely a DNS system.

2. Discovery and Timing Observations

We first detected PSR J1759+5036 in single-pulse search output from the discovery observation of PSR J1800+5034, an unrelated 578 ms pulsar with a DM of 22.7 pc cm^{-3} published in 2018 (Lynch et al. 2018). The single pulses were detected at a DM of 7.77 pc cm^{-3} two years after timing observations ceased for the former source. The pulsar was subsequently detectable in a periodicity search with a spin period of 176 ms, and timed using the archival data of the PSR J1800+5034 observation campaign, consisting of 24 observations taken on the GBT from February 2013 to January 2014 at 820 MHz with time resolution of 81.92 μs and 2048 frequency channels. Dedispersing at the DM of 7.77 pc cm^{-3} and refolding at the 176 ms spin period of PSR J1759+5036 produced 10 detections. As PSR J1759+5036 was not the source of interest for these observations, it was not at the center of the beam when data were being taken, possibly reducing the detected flux.

The entire timing dataset for PSR J1759+5036 spans 2013–2020 with 109 total observations of which 50 were detections. Observations at both frequencies ranged from 3 to 60 minutes. A summary of the timeline of observation runs can be found in Table 1. For all observations, the Green Bank Ultimate Pulsar Processing Instrument backend was used, and radio frequency interference (RFI) was excised using the `pazi` tool in the `PSRCHIVE` software package.[21] We then summed each observation in the time and frequency domain to generate best profiles to compute times of arrival (TOAs) using the tool `pat`. For most observations, we calculated 4–7 TOAs, depending on detection signal-to-noise ratio (S/N), with a few marginal detections only producing 1–3 useful TOAs. We made composite profiles for 350 and 820 MHz data (Figure 1) by adding together all the observations of a particular frequency using the `psradd` tool. We then used `paas` to generate a standard profile, which was then used to recalculate TOAs in order to refine the timing ephemeris.

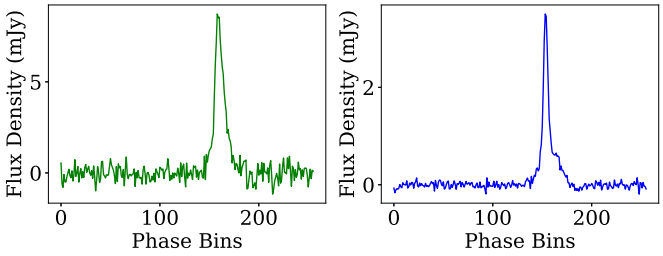

Figure 1. Composite profiles of PSR J1759+5036 at 350 (left) and 820 (right) MHz with integration times of 4.2 hr and 6.4 hr, respectively. Both profiles have 256 phase bins and were used as standard profiles to recalculate TOAs in order to refine the timing ephemeris.

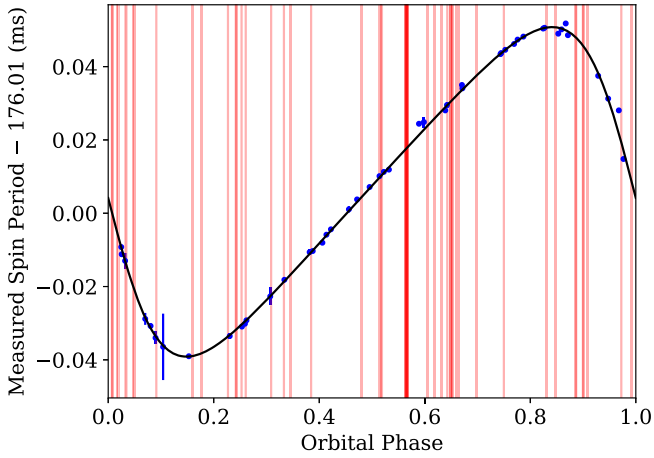

Figure 2. The observed Doppler-modulated P of each epoch vs orbital phase. Red lines signify epochs of non-detection and do not appear to be associated with any particular phase of orbit. Overlaid in black is a calculated model of the variation of P across the orbital phase. Orbital phases have been calculated in reference to the epoch of periastron.

From 2017–2019 we obtained 54 observations of PSR J1759+5036 on the GBT at 820 MHz with 40.96 μs time resolution and 2048 frequency channels. Initial timing efforts were complicated by the fact that the pulsar is in a binary system, and was also undetectable at 34 of the 54 epochs. We do not believe that extrinsic factors, such as RFI, were significant contributors to the lack of detections. Since timing required initial estimates of the Keplerian binary parameters, we measured the barycentric P at each epoch, and used methods from Bhattacharyya & Nityananda (2008) to calculate rough approximations. These were then refined using `Tempo`[22] to build a phase-connected timing solution and to study the intermittent nature of the detections. We show in Figure 2 that there is no apparent connection between the binary orbital

[21] http://psrchive.sourceforge.net/
[22] https://sourceforge.net/projects/tempo/

Table 2
Timing Solution for PSR J1759+5036

Measured Parameter	Value
R.A. (J2000)	17:59:45.672(3)
Decl. (J2000)	+50:36:56.96(2)
P (s)	0.17601634721733(8)
$\dot{P}$ (s s^{-1})	$2.43(3) \times 10^{-19}$
Dispersion Measure (pc cm^{-3})	7.775(3)
Statistic and Model Parameters	
Timing Data Span (MJD)	56,406–58,859
RMS Residual (μs)	246.54
EFAC	1.251
Number of TOAs	187
Binary Model	DD
Solar System Ephemeris	DE436
Reference Epoch (MJD)	57,633
Binary Parameters	
Orbital Period, P_b (days)	2.04298385(3)
Orbital Eccentricity, e	0.30827(12)
Projected Semi-Major Axis (lt s)	6.82461(3)
Longitude of Periastron, ω (deg)	92.142(2)
Epoch of Periastron (MJD)	57,633.09399(14)
Advance of Periastron, $\dot{\omega}$ (deg yr^{-1})	0.127(10)
Derived Parameters	
Surface Magnetic Field (10^9 Gauss)	9.5
Spin-down Luminosity (10^{30} erg s^{-1})	9.0
Characteristic Age (Gyr)	50
Dist$_{DM}$ NE2001 (pc)	711
Dist$_{DM}$ YMW16 (pc)	542
Mass Function	0.081768(1)
Minimum Companion Mass ($M_\odot$)	0.7006
Total Mass ($M_\odot$)	2.62(3)
S_{350} (mJy)	0.38(8)
S_{820} (mJy)	0.11(2)
S_{1500} (mJy)	0.12(2)

Note. Timing results are reported in units of TDB. In parentheses are the TEMPO-reported uncertainties in the last significant digit. The EFAC reported was used to achieve a reduced χ^2 of 1.0. Position uncertainty is determined from the timing fit to position. The VLA observation position is consistent with timing position. We quote distances calculated with both the NE2001 (Cordes & Lazio 2003) and YMW16 Galactic electron density models (Yao et al. 2017).

phase and the epochs of non-detections. This suggests that the lack of detections is either intrinsic to the pulsar emission mechanism or due to external interstellar medium effects, such as scintillation, possibly in combination with a poorly constrained position. A discussion of the scintillation will be presented in Section 4.3.

In 2019 May and June we conducted several observations with the Karl G. Jansky Very Large Array (see Section 2.1), through which we determined a more accurate position, which was 7.″22 from our initial position (i.e., that of PSR J1800+5034). Given that the FWHM of the GBT 820 MHz receiver is only 15′, our earlier observations suffered significantly from degraded sensitivity due to a reduced gain. The offset caused a 10% and 44% reduction in sensitivity for 350 and 820 MHz observations, respectively.

We also carried out a short, high-cadence timing campaign with the GBT at 350 MHz. At this lower frequency, we had more success at detecting PSR J1759+5036 than at 820 MHz, with five of seven observations resulting in a detection. This pulsar was also observed during 350 MHz GBNCC survey observations as a test source. We conducted another high-cadence campaign at 820 MHz in 2019 December that concluded in 2020 January. This gave us an additional 15 detections out of 24 observations.

2.1. VLA Observations

We observed PSR J1759+5036 using the VLA during 2019 May and June. Since the source was previously observed to be intermittent, we scheduled four separate observations to improve our chances of detecting it. These took place on MJDs 58,614, 58,615, 58,652, and 58,655. Each session was 2.5 hr long, with about 2 hr total on the pulsar. During this time the VLA was in the B configuration, with maximum baseline length of 11 km. We acquired data using the VLA's interferometric pulsar binning mode, which averages visibility data into a number of separate pulse phase bins following a timing ephemeris. We used 32 pulse phase bins (∼5.5 ms per bin) to record data spanning 1–2 GHz, with 1 MHz frequency resolution and 5 s dump time.

The data were processed as follows: we used `sdmpy`[23] to realign the data in the pulse phase using the best available timing solution, we dedispersed at the known DM of the pulsar, and we split the original multi-bin data into separate data sets per bin as well as a bin-averaged version. All further calibration and imaging was done using the Common Astronomy Software Applications package (CASA; McMullin et al. 2007) version 5.6.2. The data were calibrated using the standard VLA CASA calibration pipeline. The flux scale was referenced to 3C286 (Perley & Butler 2017), and interferometric phases were referenced to J1740+5211. Calibration solutions were determined from the bin-averaged data set and applied to each individual bin, which were then imaged separately. By subtracting the bin-averaged data from the single-bin data, all confusing background sources are removed, resulting in an unambiguous detection of the pulsar.

The pulsar was detected in all four observations, with flux density ranging from 0.08 to 0.21 mJy on different days. While this does show some epoch-to-epoch variations, the detectability at all four epochs suggests that scintillation at these higher frequencies is in the weak scattering regime, consistent with a lack of structure in the dynamic spectra. From the brightest observation (MJD 58,614) we determined a source position of RA = 17:59:45.66 ± 0.02 s, decl. = +50:36:57.05 ± 0.″1. This observation had a synthesized beamwidth of 4.″9 by 4.″1 at a position angle of 70°. The uncertainties quoted here reflect only the statistical uncertainty due to noise in the data. It is possible that systematic effects may be present at the sub-beam level, however, this position is consistent with values obtained from the other three observations, as well as with the later-determined timing position presented in Table 2.

3. Timing Analysis

Our total data set spanned roughly seven years with a three year gap between archived timing data taken during 2013–2014 for PSR J1800+5034 and the 2017–2020 data for PSR J1759+5036. This can be seen in our timing residuals, shown in

[23] http://github.com/demorest/sdmpy

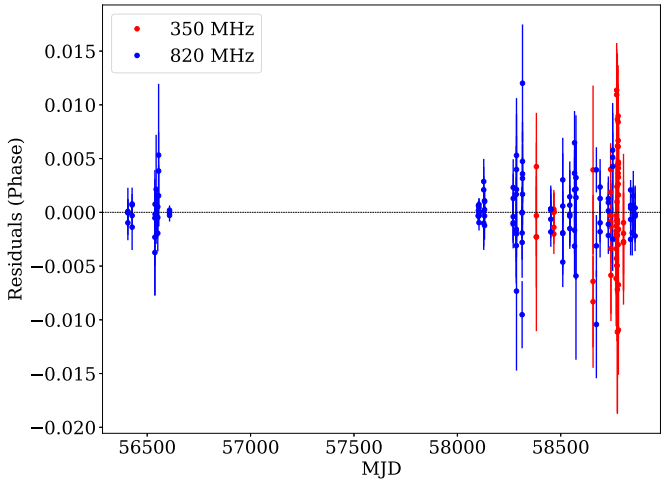

Figure 3. MJD vs post-fit residuals for 187 TOAs over 48 epochs. The TOAs from before MJD 58101 are from archived data taken from the PSR J1800 +5034 timing campaign. Red TOAs are calculated from 350 MHz data and blue TOAs are from 820 MHz data.

Figure 3. Our ephemeris, shown in Table 2, is reported in TDB units, and uses the JPL DE436 solar system ephemeris and the DD binary model (Damour & Deruelle 1985, 1986). We fit for DM by splitting five closely spaced individual observations taken at 350 MHz into four frequency subbands and computing a single TOA from each subband. Our DM measurements indicate a distance of approximately 700 pc using the NE2001 Galactic electron density model (Cordes & Lazio 2003), or 550 pc using YMW16 model of Galactic electron density (Yao et al. 2017). These distances are consistent within the errors for the two models.

We were able to measure the PK parameter advance of periastron ($\dot{\omega}$) with high significance. Our reduced χ^2 ($\chi_{\rm red}$) was initially 1.5 with 175 degrees of freedom (DOF), so we used a multiplicative error factor (EFAC) that accounts for random radiometer noise by applying a constant multiplier to all TOA error bars. Our applied EFAC was 1.25, which gave a $\chi^2_{\rm red}$ of 1.0. The root-mean-square (RMS) of our timing solution is 246 μs, or roughly 0.1% of the pulsar spin period.

We calculated the average flux density at 350 (S_{350}) and 820 (S_{820}) MHz, as seen in Table 2, using the respective composite profiles integrated across pulse phase, using the radiometer equation (Dewey et al. 1985). For S_{350}, we assumed a bandwidth of 80 MHz, a system temperature ($T_{\rm sys}$) of 46 K, and a sky temperature ($T_{\rm sky}$) of 38 K (Haslam et al. 1982). For S_{820} we assumed a bandwidth of 200 MHz, a $T_{\rm sys}$ of 29 K, and a $T_{\rm sky}$ of 4.2 K. $T_{\rm sky}$ values were calculated from the Haslam et al. (1982) sky-maps and scaled to the appropriate frequency with a spectral index of −2.6. We calculated the off-pulse noise of each profile and then used the expected radiometer noise to scale the entire profile accordingly to determine the flux density. We estimate an approximate error of 20% for each flux measurement made using the radiometer equation. From fitting a power law to the three points we get a spectral index of -1.0 ± 0.4.

3.1. Single-Pulse Analysis

Using the `PRESTO` package `single_pulse_search.py` (Ransom 2001), we searched for single pulses with S/N greater than 7 at every epoch between DMs of 0 and 20 pc cm^{-3} with match-filtered box car widths ranging of 30 times the sample size.

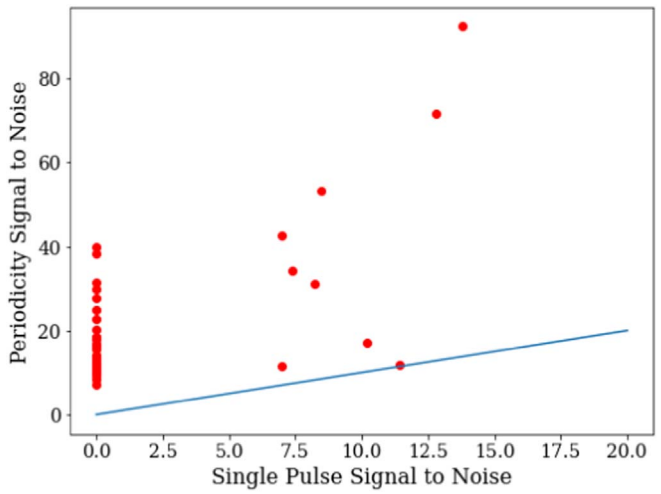

Figure 4. Folded profile periodicity search S/N vs the S/N of the brightest detectable single pulse at each epoch of the timing observations, with the line representing a slope of 1. On all days, the pulsar is equally or better detected in a periodicity search. Here, a value of zero indicates the pulse was not detectable using that method. The original detection is omitted in this plot.

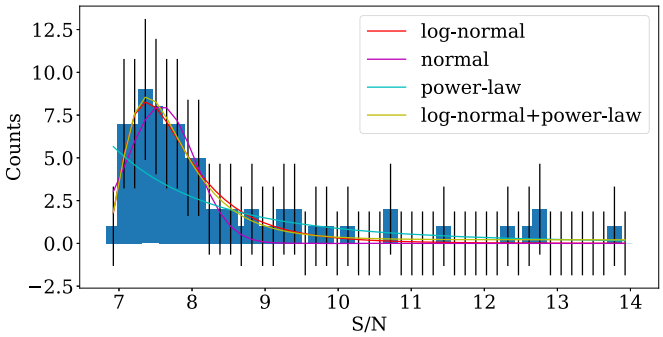

Figure 5. Histogram of the S/N of single pulses with 1σ error bars, using a minimum S/N cutoff of 7. Overlaid are the log-normal, normal, power-law, and log-normal plus power-law distributions that were fit to the data.

We determined whether pulses were indeed from PSR J1759+5036 and not due to RFI by first requiring that the S/N be modeled as a Gaussian distribution with peak S/N at a dispersion measures DM between 7 and 8.25 pc cm^{-3}, a range determined by the distribution of measured (DMs) on the detectable epochs. Through this method we found that 20% of observations showed detectable single pulses. We did not observe any clear difference in the rate of single pulse detection for different observing frequencies.

Since this pulsar was originally detected only through its single pulses, we explored whether it is typically better detected in this way. In Figure 4 we show the ratio of the S/N of the composite profile along with the S/N of the brightest single pulse. This shows that PSR J1759+5036 is almost always detected at higher S/N values through periodicity searches than through single pulses, indicating that it is not an RRAT (Shapiro-Albert et al. 2018). We ran the single-pulse search on the entire dataset, and only in the first search observation was the pulsar detected only through single pulses.

We also wanted to see if the single pulse S/N distribution had a power-law tail, like those seen in RRATs and systems that emit giant pulses (Mickaliger et al. 2018). In Figure 5, we show a histogram of the detected single-pulse S/N values recorded at a central frequency of 820 MHz. We show 1σ error bars as calculated in Gehrels (1986). To study the behavior of

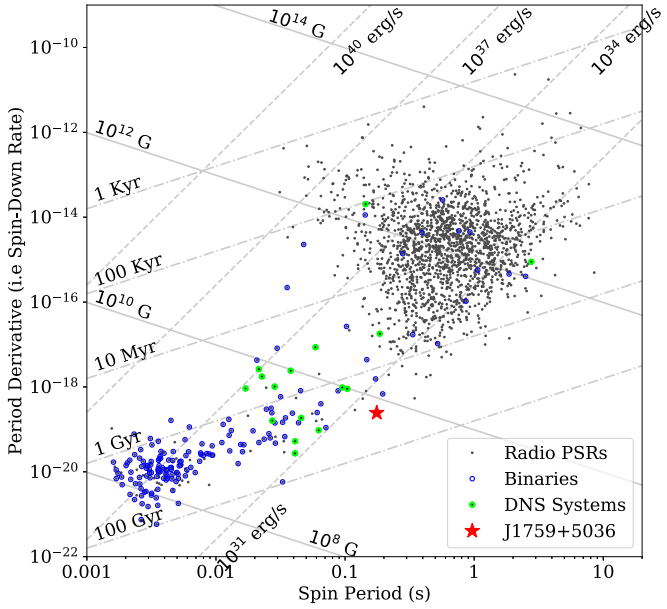

Figure 6. P vs. $\dot{P}$ of all known pulsars, with binary pulsars in blue, DNS systems in green, and PSR J1759+5036 in red. The parallel lines correspond to constant values of the characteristic age (dashed–dotted), spin-down energy loss rate (dashed), and surface dipole inferred magnetic field (solid); (see, e.g., Lorimer & Kramer 2012 for definitions).

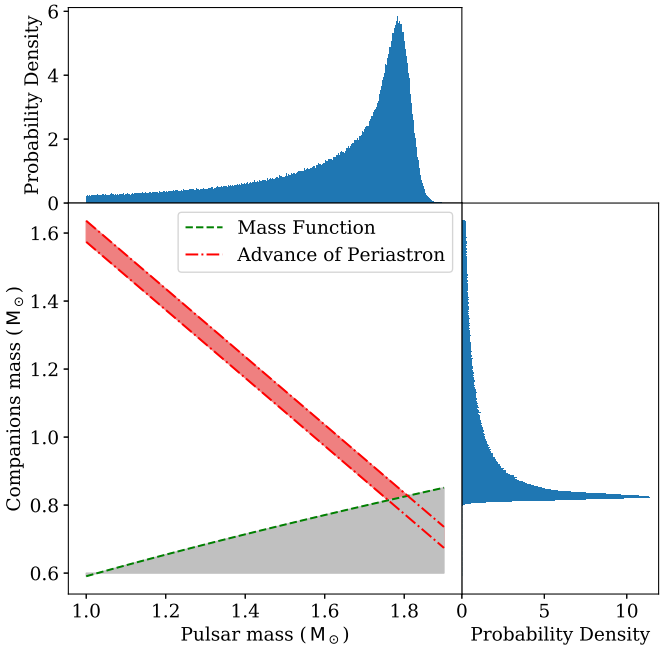

Figure 7. Allowed values of pulsar mass vs companion mass given the rate of advance of periastron (between the red dashed lines) and the mass function (above the green dotted line). The red shaded region indicates possible values of pulsar mass and companion mass. Above and to the right are the probability distributions for the pulsar and companion mass, respectively.

the S/N amplitudes we fit log-normal, normal, power-law, and combined log-normal/power-law distributions to the data. Given the large error bars on each bin, all four fits had low chi-squared values, but due to the low number of counts per bin we cannot make any firm conclusions. With future datasets we may be able to distinguish between these models and better understand how the single-pulse properties of this pulsar compare to those of other pulsars and RRATs.

4. Discussion

The small $\dot{P}$ and relatively large P place PSR J1759+5036 in a sparsely populated region of P and $\dot{P}$ space (see Figure 6). The relatively low magnetic field of about 10^{10} G suggests that this pulsar is partially recycled, but some process halted accretion from the companion before spin-up to very short periods. The observed high eccentricity is likely an artifact of the companion supernova explosion, and is consistant with those seen in DNS systems (Tauris et al. 2017; Pol et al. 2019).

The time to merger due to gravitational wave radiation is 182 Gyr, much longer than a Hubble time, meaning that PSR J1759+5036's discovery will not impact DNS merger rate estimates (Lorimer 2008; Pol et al. 2019).

4.1. Nature of the Binary System

The mass function implies a minimum companion mass of $0.7\,M_\odot$, assuming a system inclination of 90° (Lorimer 2008). Our measurement of $\dot{\omega}$ corresponds to a total system mass of $2.62 \pm 0.03\,M_\odot$. In Figure 7 we have overlaid the possible pulsar and companion masses allowed by $\dot{\omega}$ with those forbidden by the mass function. This allowed us to determine the maximum pulsar mass to be $1.8\,M_\odot$. The probability distributions for pulsar and companion mass in the figure have been calculated using the measured $\dot{\omega}$ assuming random orbital inclinations. The 2σ mass ranges are 1.26–1.79 $M_\odot$ for the pulsar and 0.84–1.37 $M_\odot$ for the companion, with a 0.16 probability that the companion mass is greater than $1.2\,M_\odot$. If the companion is indeed a NS, as seems likely given its spindown and orbital properties, the inclination angle must be less than 44° (assuming the NS mass must be greater than $1.2\,M_\odot$ (Thorsett & Chakrabarty 1999).

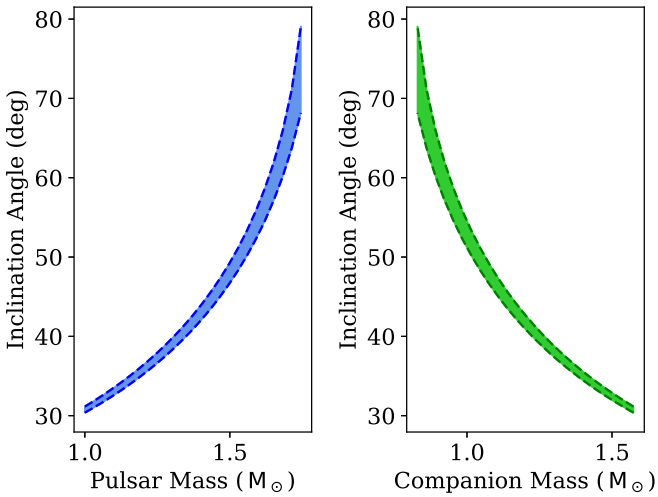

Figure 8. Left: Potential pulsar masses vs projected inclination angle implied by each mass as shown by the shaded region. Right: Potential masses of the companion mass vs inclination angle, with the shaded region indicating possible values.

In Figure 8 we show projected values for the inclination angle of the binary system using the range of possible pulsar and companion masses determined by the total system mass and the mass function. We can infer from this that the inclination angle must be between 35° and 75°.

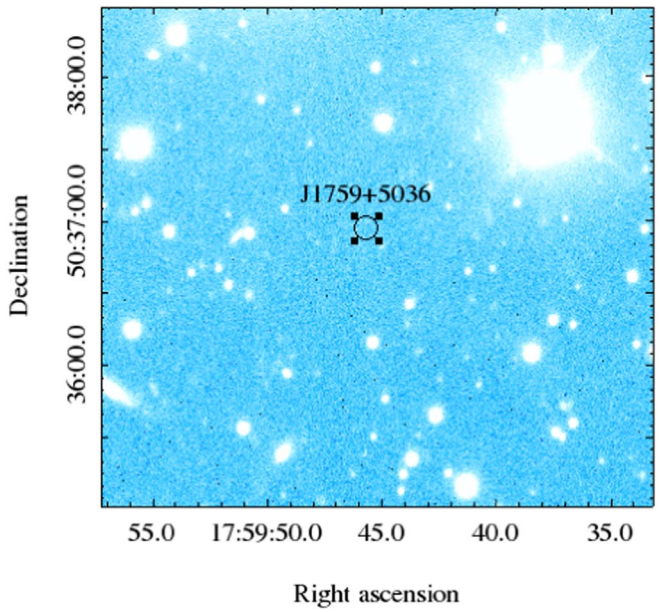

Figure 9. Image from the LCO observation to look for an optical counterpart for PSR J1759+5036. The black circle represents a 5″ diameter region around the pulsar, much larger than the <1″ error in position.

4.2. Optical Constraints on a Companion

We conducted optical observations with the Las Cumbres Observatory 2 meter telescope on Haleakala on 30 April 2020. Three consecutive 500 s exposures were taken with the SDSS r' filter (median MJD 58969.5637447) and then another three 500s exposures with the SDSS g' filter (median MJD 58969.5457716). These were then median added for each filter and aperture photometry was attempted on them. We used images whose dark subtraction, bias correction, flat-fielding, and plate solutions were generated by the LCO *Banzai* pipeline. In neither filter was a counterpart detected at the position of the pulsar (Figure 9). By measuring the faintest nearby stars using two SDSS catalog (release 12) stars as references, we estimate a limiting magnitude of ∼23.5 in both filters at the position of PSR J1759+5036.

Using 23.5 as an apparent magnitude minimum limit for a possible WD companion, we determined temperature and age limits for distances of 500, 700, and 1000 pc to account for the uncertainty in the DM distance. In Figure 10, we have plotted WD cooling curves,[24] with the limits for each distance indicated (Bergeron et al. 1995; Holberg & Bergeron 2006; Kowalski & Saumon 2006; Bergeron et al. 2011; Tremblay et al. 2011; Blouin et al. 2018; Bédard et al. 2020). For this analysis we assumed a hydrogen WD atmosphere, used dustmaps to take extinction into account, and used cooling curves for masses of 0.8 $M_\odot$ and 1.2 $M_\odot$, which are the lower and upper mass limits for a WD companion for this system (Tremblay et al. 2011). For a 0.8 $M_\odot$ companion at a distance of 700 pc the effective temperature is <6600 K and the age is >3.5 Gyr, which is based on the more constraining g' limit. At the same distance, for a 1.2 $M_\odot$ companion, the effective temperature <9700 K and the age >2.6 Gyr. These limits are not particularly constraining as, if the companion has nearly the same age as the pulsar, it would have a temperature below either of these limits (see Figure 10) and likely be too faint to be detected even with deeper optical observations.

[24] http://www.astro.umontreal.ca/~bergeron/CoolingModels/

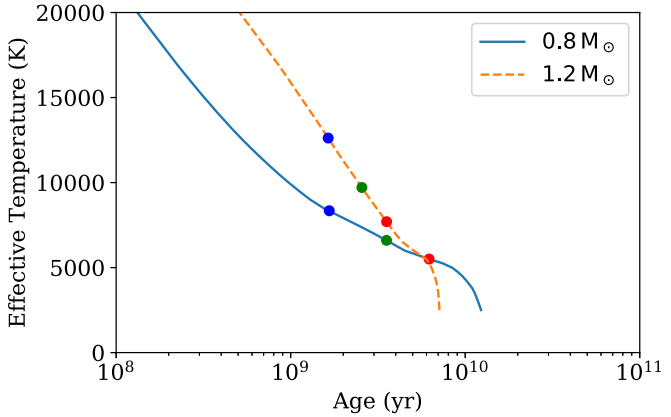

Figure 10. Cooling curves for 0.8 $M_\odot$(blue) and 1.2 $M_\odot$(orange) WD stars with effective temperature upper limits of and age lower limits indicated for distances of 500 pc (red), 700 pc (green), and 1000 pc (blue). For an 0.8 $M_\odot$ WD we have limits of <5500 K and >6.2 Gyr at 500 pc, <6600 K, and >3.5 Gyr at 700 pc, and <8400 K and >6.2 Gyr at 500 pc. For a 1.2 $M_\odot$ WD we have limits of <7700 K and >3.5 Gyr at 500 pc, <9700 K and >2.6 Gyr at 700 pc, and <12,600 K and >1.6 Gyr at 500 pc.

Being unable to detect an optical counterpart at the position of PSR J1759+5036, we have ruled out a main-sequence star companion (already very unlikely due to the tight orbit) and most white dwarf (WD) stars (Figure 9). Any main sequence star of comparable luminosity and size to the Sun at our DM estimated distances (Table 2) would have a magnitude of 13–15 and thus would be easily visible. Optical observations at a magnitude of 26–27 would be needed to confidently rule out or confirm a WD companion.

While most pulsar-WD binaries are circular, there are several systems with eccentric companions, such as PSR J2305 + 4707 and PSR J1755−2550. However, these binaries have some significant differences in properties from PSR J1759+5036. Both have limited evidence of recycling and have significantly lower characteristic ages of 29.7 Myr and 2.1 Myr, respectively, whereas PSR J1759+5036 shows evidence of partial recycling and a much larger characteristic age (Ng et al. 2018; van Kerkwijk & Kulkarni 1999). Therefore, we argue it is most likely a DNS system.

4.3. Intermittency

The low DM of PSR J1759+5036 suggests that diffractive interstellar scintillation may play a role in the intermittency we observed, shown in Figure 2. To study this, we created dynamic spectra of each detected epoch by first folding the data in time sub-integrations of 60 s using the `fold_psrfits` package from `PSRCHIVE` (van Straten et al. 2012). Then, we used `pam` to fold the data into frequency sub-integrations of 3 MHz and plotted the intensity of each frequency/time bin and corrected the bandpass for instrument variation using the python package `PyPulse` (Lam 2017). In Figure 11 we have shown dynamic spectra from two epochs where scintillation was observed.

The NE2001 electron density model predicts a scintillation bandwidth of ∼26 at 350 MHz and ∼40 at 820 MHz at the position and DM of J1759+5036 (Cordes & Lazio 2003).

Given the measured timing residual and the six year baseline of our timing data, we can place an upper limit on the transverse velocity of 16 km s^{-1}. This is rather low, but consistent with other DNS systems such as PSR J0737-3039A/B (∼9 km s^{-1})

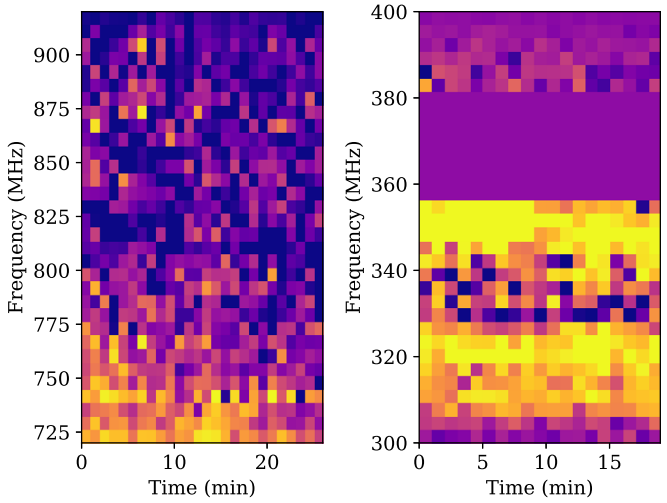

Figure 11. Left: A dynamic spectrum on epoch 58131 at 820 MHz. Intensity is plotted against frequency bins of roughly 6 MHz, and time bins of 60 s. Right: Dynamic spectrum on epoch 58466 at 350 MHz. On-pulse intensity is plotted vs frequency and time, with time bins of 60 s and frequency bins of roughly 3 MHz. The purple strip between 360 and 380 MHZ is a region of bright RFI that was removed from the data.

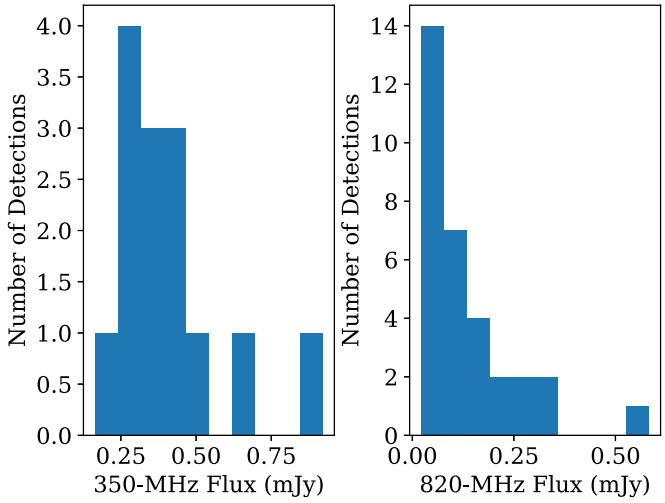

Figure 12. The distribution of flux densities measured at each epoch at 350 MHz (left) and 820 MHz (right). Flux densities that were calculated from observations impacted by the position offset were corrected to reflect the degraded sensitivity.

and PSR B1913+16 ($\sim$22 km s^{-1}) (Deller et al. 2009, 2018). For this velocity we estimate a scintillation timescale of $\sim$6400 s at 350 MHz and $\sim$9300 s at 820 MHz. Since these timescales are significantly longer than any of our observations this is consistent with our inability to resolve scintles in time.

On epoch 58466, we resolved two scintles in frequency with the more visible scintle having a bandwidth of roughly 25 MHz, indicating that the NE2001 prediction is accurate (Figure 11). The second scintle is not fully resolved due to RFI excision. For the 820 MHz data we were unable to fully resolve scintles on any of the epochs, but on one epoch, MJD 58131, we detected a partially resolved scintle that is cut off at the edge of the receiver band (Figure 11). It is easy to see that this epoch may have resulted in a non-detection if this scintle was centered at a slightly lower frequency. Thus, scintillation may explain the numerous non-detections of this pulsar at 820 MHz.

On one epoch, MJD 58772, PSR J1759+5036 was only detected in the second and third of three contiguous observations. The first observation was six minutes, the second was 30 minutes, and the third was five minutes. There was a two minute gap between the first two observations and a ten minute gap between the second and third observations. The first detection was strong, with an S/N of 17.2, whereas the second had an S/N of 9.6. These timescales are consistent with those expected due to scintillation, and is further evidence that scintillation may be responsible for the nondetections.

In Figure 12, we show histograms of the flux variations at both 350 and 820 MHz. The 820 MHz distribution shows the exponential tail expected for variability due to diffractive interstellar scintillation (Scheuer 1968; Hesse & Wielebinski 1974). Flux densities that would have been impacted by the position offset in our earlier observations have been corrected to reflect the degraded sensitivity.

We ran a Lomb–Scargle analysis (e.g., Scargle 1982; Palliyaguru et al. 2011) to determine if there was any periodicity to the on and off periods of PSR J1759+5036, shown in Figure 13. The analysis tested 122 trial periods ranging from 50–2530 days, and the most significant signal had a periodicity of 171 days with a false alarm probability of 0.05. This is only marginally significant; more data are needed to determine whether a true periodicity might exist.

5. Conclusions and Future Work

In this paper we report on the discovery and timing campaign for PSR J1759+5036, a 176 ms binary pulsar with a 2.04-day eccentric orbit about a likely neutron star companion. Over our seven year dataset, this pulsar has been highly intermittent with an approximately 45% detection rate, which we believe to be largely attributed to scintillation, possibly combined with a poorly constrained position that we then determined through observations taken with the VLA.

We were able to measure all five Keplerian parameters as well as a single PK parameter, $\dot{\omega}$. This allowed us to determine the minimum companion mass and total system mass, which we used to place limits on possible pulsar and companion masses as well as system inclination angle. Due to the eccentricity (0.308) of the system and lack of optical counterpart, we believe the candidate is most likely a neutron star. We have ruled out a main sequence companion and most white dwarf stars (see Section 4.2).

Continued follow-up observations and timing of PSR J1759+5036 are expected to eventually produce a measurement of a second PK parameter, which would allow us to fully constrain the pulsar and companion masses. Using simulated TOAs, we estimate that approximately 12 years of data would be needed to measure γ, the time dilation, and the gravitational redshift parameter, which would also determine the inclination angle of the system. We also hope to be able to measure the proper motion, which would allow us to calculate more accurate estimates of distance and pulsar velocity. Currently, follow-up observations are being conducted on the Canadian Hydrogen Intensity Mapping Experiment telescope with weekly cadence, the results from which are expected to be included in future publications.

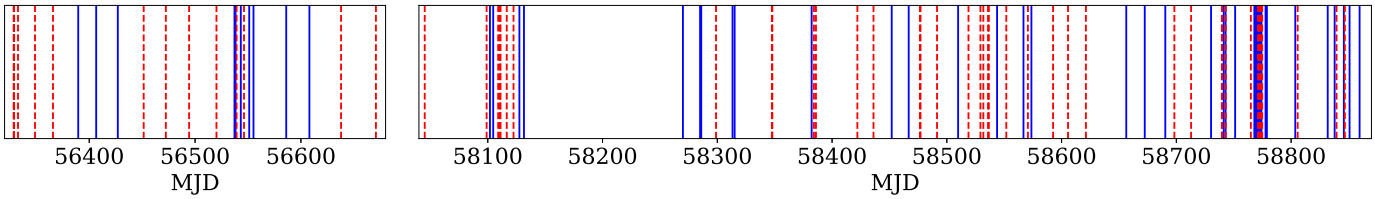

Figure 13. Epochs of observation on which PSR J1759+5036 was detected (blue sold lines) and not detected (red dotted lines). Left: 2013–2014 data set. Right: 2017–2020 data set.

M.A.M., J.K.S., H.B., M.D., P.B.D., W.F., E.F., D.L.K., R.S.L., A.E.M., S.M.R., A.S., C.S., X.S., I.H.S., and M.S. are members of the NANOGrav Physics Frontiers Center, supported by NSF award number 1430284. V.M.K. holds the Lorne Trottier Chair in Astrophysics and Cosmology, a Distinguished James McGill Chair, and receives support from an NSERC Discovery Grant, the Herzberg Award, CIFAR, and from the FRQ-QNT Centre de Recherche en Astrophysique du Quebec. M.A.M., G.Y.A., and M. G.M. are also supported by NSF award number 1458952. We thank the WVU Research Corporation for their purchase of observing time on the GBT, which has supported some of the observations for this project. Pulsar work at UBC is supported by an NSERC Discovery Grant and by the Canadian Institute for Advanced Research. The National Radio Astronomy Observatory and Green Bank Observatory are facilities of the National Science Foundation operated under cooperative agreement by Associated Universities, Inc. Computations were made on the supercomputer Guillimin at McGill University[25], managed by Calcul Quebec and Compute Canada. The operation of this supercomputer is funded by the Canada Foundation for Innovation (CFI), NanoQuebec, RMGA and the Fonds de recherche du Quebec —Nature et technologies (FRQ-NT). VLA observations were taken as project 19A-387. GBT observations were taken under projects AGBT13A-458, AGBT17B-285, AGBT17B-423, AGBT17B-292, AGBT18A-482, AGBT17B-325, AGBT18B-335, AGBT18B-360, AGBT19A-180, AGBT19A-486, AGBT19B-306, AGBT19B-327, and AGBT19B-320.

Facilities: Robert C. Bryd Green Bank Telescope (GBT), Karl G. Jansky Very Large Array (VLA), Las Cumbres Observatory (LCO).

Software: `Astropy` (Price-Whelan et al. 2018), `PRESTO` (Ransom 2001), `PSRCHIVE`(van Straten et al. 2012), `PINT` (Luo et al. 2021), `NumPy` (Harris et al. 2020), `PyPulse` (Lam 2017), `TEMPO`,`SciPy`, `CASA` (McMullin et al. 2007), `DS9` (Joye & Mandel 2003), `sdmpy` (http://github.com/demorest/sdmpy).

ORCID iDs

G. Y. Agazie https://orcid.org/0000-0001-5134-3925
M. A. McLaughlin https://orcid.org/0000-0001-7697-7422
J. K. Swiggum https://orcid.org/0000-0002-1075-3837
D. L. Kaplan https://orcid.org/0000-0001-6295-2881
H. Blumer https://orcid.org/0000-0003-4046-884X
P. Chawla https://orcid.org/0000-0002-3426-7606
M. DeCesar https://orcid.org/0000-0002-2185-1790
P. B. Demorest https://orcid.org/0000-0002-6664-965X
W. Fiore https://orcid.org/0000-0001-5645-5336
E. Fonseca https://orcid.org/0000-0001-8384-5049
J. D. Gelfand https://orcid.org/0000-0003-4679-1058
V. M. Kaspi https://orcid.org/0000-0001-9345-0307
V. I. Kondratiev https://orcid.org/0000-0001-8864-7471
J. van Leeuwen https://orcid.org/0000-0001-8503-6958
L. Levin https://orcid.org/0000-0002-2034-2986
E. F. Lewis https://orcid.org/0000-0002-2972-522X
R. S. Lynch https://orcid.org/0000-0001-5229-7430
A. E. McEwen https://orcid.org/0000-0001-5481-7559
H. Al Noori https://orcid.org/0000-0002-4187-4981
E. Parent https://orcid.org/0000-0002-0430-6504
S. M. Ransom https://orcid.org/0000-0001-5799-9714
A. Schmiedekamp https://orcid.org/0000-0003-4391-936X
C. Schmiedekamp https://orcid.org/0000-0002-1283-2184
X. Siemens https://orcid.org/0000-0002-7778-2990
R. Spiewak https://orcid.org/0000-0002-6730-3298
I. H. Stairs https://orcid.org/0000-0001-9784-8670
M. Surnis https://orcid.org/0000-0002-9507-6985

[25] www.hpc.mcgill.ca

References

Alpar, M. A., Cheng, A. F., Ruderman, M. A., & Shaham, J. 1982, Natur, 300, 728
Bédard, A., Bergeron, P., Brassard, P., & Fontaine, G. 2020, ApJ, 901, 93
Bergeron, P., Wesemael, F., & Beauchamp, A. 1995, PASP, 107, 1047
Bergeron, P., Wesemael, F., Dufour, P., et al. 2011, ApJ, 737, 28
Bhattacharyya, B., & Nityananda, R. 2008, MNRAS, 387, 273
Blouin, S., Dufour, P., & Allard, N. F. 2018, ApJ, 863, 184
Cordes, J. M., & Lazio, T. J. W. 2003, NE2001. II. Using Radio Propagation Data to Construct a Model for the Galactic Distribution of Free Electrons, arXiv:astro-ph/0301598
Damour, T., & Deruelle, N. 1985, Ann. Inst. Henri Poincaré Phys. Théor, 43, 107
Damour, T., & Deruelle, N. 1986, Ann. Inst. Henri Poincaré Phys. Théor, 44, 263
Damour, T., & Taylor, J. H. 1992, PhRvD, 45, 1840
Deller, A. T., Bailes, M., & Tingay, S. J. 2009, Sci, 323, 1327
Deller, A. T., Weisberg, J. M., Nice, D. J., & Chatterjee, S. 2018, ApJ, 862, 139
Dewey, R. J., Taylor, J. H., Weisberg, J. M., & Stokes, G. H. 1985, ApJL, 294, L25
Gehrels, N. 1986, ApJ, 303, 336
Harris, C. R., Jarrod Millman, K., van der Walt, S. J., et al. 2020, Natur, 585, 357
Haslam, C. G. T., Salter, C. J., Stoffel, H., & Wilson, W. E. 1982, A&AS, 47, 1
Hesse, K. H., & Wielebinski, R. 1974, A&A, 31, 409
Holberg, J. B., & Bergeron, P. 2006, AJ, 132, 1221
Joye, W. A., & Mandel, E. 2003, in ASP Conf. Ser. 295, Astronomical Data Analysis Software and Systems XII, ed. R. I. Payne, R. I. Jedrzejewski, & R. N. Hook (San Francisco, CA: ASP), 489
Kowalski, P. M., & Saumon, D. 2006, ApJL, 651, L137
Kramer, M., Stairs, I. H., Manchester, R. N., et al. 2006, Sci, 314, 97
Lam, M. T. 2017, PyPulse: PSRFITS handler
Lorimer, D. R. 2008, LRR, 11, 8
Lorimer, D. R., Bailes, M., McLaughlin, M. A., Narkevic, D. J., & Crawford, F. 2007, Sci, 318, 777
Lorimer, D. R., & Kramer, M. 2012, Handbook of Pulsar Astronomy (Cambridge: Cambridge University Press)
Luo, J., Ransom, S., Demorest, P., et al. 2021, ApJ, 911, 45
Lynch, R. S., Swiggum, J. K., Kondratiev, V. I., et al. 2018, ApJ, 859, 93

Manchester, R. N., Hobbs, G. B., Teoh, A., & Hobbs, M. 2005, VizieR Online Data Catalog,, VII/245
McEwen, A. E., Spiewak, R., Swiggum, J. K., et al. 2020, ApJ, 892, 76
McLaughlin, M. A., Lyne, A. G., Lorimer, D. R., et al. 2006, Natur, 439, 817
McMullin, J. P., Waters, B., Schiebel, D., Young, W., & Golap, K. 2007, in ASP Conf. Ser. 376, Astronomical Data Analysis Software and Systems XVI, ed. F. Hill & D. J. Bell (San Francisco, CA: ASP), 127
Mickaliger, M. B., McEwen, A. E., McLaughlin, M. A., & Lorimer, D. R. 2018, MNRAS, 479, 5413
Ng, C., Kruckow, M. U., Tauris, T. M., et al. 2018, MNRAS, 476, 4315
Palliyaguru, N. T., McLaughlin, M. A., Keane, E. F., et al. 2011, MNRAS, 417, 1871
Perley, R. A., & Butler, B. J. 2017, ApJS, 230, 7
Phinney, E. S. 1992, Philosophical Transactions: Physical Sciences and Engineering, 341, 39
Pol, N., McLaughlin, M., & Lorimer, D. R. 2019, ApJ, 870, 71
Price-Whelan, A., Crawford, S., Sipocz, B., et al. 2018, Astropy/Astropy-V2.0-Paper: Final Draft, Zenodo
Ransom, S. M. 2001, PhD Thesis, Harvard Univ.
Scargle, J. D. 1982, ApJ, 263, 835
Scheuer, P. A. G. 1968, Natur, 218, 920
Shapiro-Albert, B., McLaughlin, M., & Keane, E. 2018, ApJ, 866, 152
Stairs, I. H. 2003, LRR, 6, 5
Stovall, K., Lynch, R. S., Ransom, S. M., et al. 2014, ApJ, 791, 67
Tauris, T. M., Kramer, M., Freire, P. C. C., et al. 2017, ApJ, 846, 170
Taylor, J. H., & Weisberg, J. M. 1989, ApJ, 345, 434
Thornton, D., Stappers, B., Bailes, M., et al. 2013, Sci, 341, 53
Thorsett, S. E., & Chakrabarty, D. 1999, ApJ, 512, 288
Tremblay, P. E., Bergeron, P., & Gianninas, A. 2011, ApJ, 730, 128
van Kerkwijk, M. H., & Kulkarni, S. R. 1999, ApJL, 516, L25
van Straten, W., Demorest, P., & Osłowski, S. 2012, Pulsar data analysis with PSRCHIVE, arXiv:1205.6276
Yao, J. M., Manchester, R. N., & Wang, N. 2017, ApJ, 835, 29